

High efficacy of tamoxifen-loaded L-lysine coated magnetic iron oxide nanoparticles in cell cycle arrest and anti-cancer activity for breast cancer therapy

Soheila Rostami¹, Farzaneh Tafvizi^{1*}, Hamid Reza Kheiri Manjili²

¹Department of Biology, Parand Branch, Islamic Azad University, Parand, Iran

²Zanjan Pharmaceutical Nanotechnology Research Center, Zanjan University of Medical Sciences, Zanjan, Iran

Article Info



Article Type:
Original Article

Article History:

Received: 11 Aug. 2020

Revised: 10 Oct. 2020

Accepted: 14 Nov. 2020

ePublished: 1 Dec. 2021

Keywords:

Magnetic iron oxide nanoparticles, L-lysine, Tamoxifen, MCF-7 cell line, Apoptosis

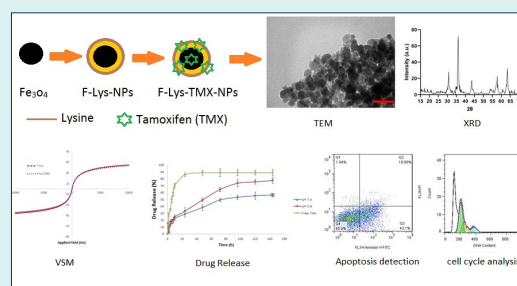
Abstract

Introduction: Due to the side effects of drugs, the development of nanoscale drug delivery systems has led to a significant improvement in medicinal therapies due to drug pharmacokinetics changes, decreased toxicity, and increased half-life of the drug. This study aimed to synthesize tamoxifen (TMX)-loaded L-lysine coated magnetic iron oxide nanoparticles as a nano-carrier to investigate its cytotoxic effects and anti-cancer properties against MCF-7 cancer cells.

Methods: Magnetic Fe_3O_4 nanoparticles were synthesized and coated with L-lysine (F-Lys NPs). Then, TMX was loaded onto these NPs. The characteristics of synthesized nanoparticles (F-Lys-TMX NPs) were evaluated by X-ray diffraction (XRD), Fourier-transform infrared spectroscopy (FTIR), scanning electron microscopy (SEM), transmission electron microscopy (TEM), dynamic light scattering (DLS), differential scanning calorimetry (DSC), vibrating sample magnetometer (VSM), and thermogravimetric analysis (TGA). The drug release was analyzed at pH 5.8 and pH 7.4. The MCF-7 cells were exposed to F-Lys-TMX NPs, F-Lys NPs, and TMX for 24, 48, and 72 hours. To evaluate the cytotoxic potential of designed nanoparticles, MTT and apoptosis assays, real-time PCR, and cell cycle analysis was carried out.

Results: The F-Lys-TMX NPs had spherical morphology with a size ranging from 9 to 30 nm. By increasing the nanoparticles concentration and treatment time, more cell proliferation inhibition and apoptosis induction were observed in F-Lys-TMX NPs-treated cells compared to the TMX. The expression levels of ERBB2, cyclin D1, and cyclin E genes were down-regulated and expression levels of the caspase-3 and caspase-9 genes were up-regulated. Studies on the drug release revealed a slow and controlled pH-dependent release of the nanoparticles. Cell cycle analysis indicated that F-Lys-TMX NPs could arrest the cells at the G0/G1 phase.

Conclusion: The findings suggest that F-Lys-TMX NPs are more effective and have the potential for cell proliferation inhibition and apoptosis induction compared to the TMX. Hence, F-Lys-TMX NPs can be considered as an anti-cancer agent against MCF-7 breast cancer cells.



Introduction

Breast cancer (BC) is the most common cancer in women.¹ The death rate of BC is 33.21 per 100 000 according to the national databases. As stated by Iran statistics, BC rates have been reported to be 14.2 per 100 000.²

The incidence of BC in Iran is at least one decade earlier than in women in developed countries. The average age at BC diagnosis in Western countries and Iran are 56 and 45

years old, respectively. Depending on the stage, place, the tumor progress, and the patient's condition, a combination of different therapeutic modalities is used.³

Common therapies for BC are surgery, chemotherapy, and radiotherapy, each can lead to hypoxia in varying degrees.³

Tamoxifen (TMX) is widely used in all stages of BC. TMX is prescribed in the treatment of hormone-



*Corresponding author: Farzaneh Tafvizi, Email: farzanehtafvizi54@gmail.com, f.tafvizi@rkiau.ac.ir



© 2022 The Author(s). This work is published by BioImpacts as an open access article distributed under the terms of the Creative Commons Attribution Non-Commercial License (<http://creativecommons.org/licenses/by-nc/4.0/>). Non-commercial uses of the work are permitted, provided the original work is properly cited.

dependent cancers. It prevents activation of the receptor in the tissue by endogenous estrogens as an antagonist.⁴ The side effects of this drug include hot flashes, vaginal bleeding, insomnia, menopause, vaginal pruritus, digestive disorders, tumor inflammation, fluid retention, baldness, uterus fibroids, visual disturbances (corneal changes, cataracts, and retinopathy), platelets or white blood cells reduction, rarely reduced neutrophils and changes in the liver enzymes.^{5,6}

Chemotherapy drugs including TMX, cause drug resistance in addition to many side effects.⁷ The cells pump the drug out of the cell by overexpression of anti-apoptotic, stress-response proteins and drug efflux ABC transporters. Drug resistance also increases drugs dosage usage, resulting in more toxicity to normal organs and tissues.⁸⁻¹⁰

Therefore, drug targeting systems have been improved using nanotechnology to reduce the systemic distribution of drugs and their side effects.^{11,12}

Nano-delivery vehicles have several benefits in cancer treatment due to their small size, protective system to enhance drug stability, surface features for the target localization, and narrow size distribution.^{13,14} In addition, nanomaterials are able to penetrate the cells by active and inactive endocytosis.^{15,16}

Magnetic nanoparticles are commonly used in the targeted delivery of therapeutic agents and perform based on the magnetic drug targeting, which includes a strong tendency between the ligand and the receptor, or through the particular tissue magnetic absorption.¹⁷

Among various nanoparticles, iron oxide nanoparticles (IONPs) are remarkable because of their paramagnetic behavior and low cost.¹⁸ Another advantage of IONPs is that they are degraded, metabolized, and do not accumulate in the body.¹⁹

Magnetic iron oxide nanoparticles (MIONPs) are known as useful nano-materials with high efficiency. They have a number of applications, including drug delivery,²⁰ cell labeling,²¹ magnetic resonance imaging,²² and antibacterial activity.²³ Despite the unique properties of these nanoparticles, they can be conjugated to different materials and used in targeted therapies.^{24,25} Due to the high surface energy of MIONPs, they can aggregate and may interact with plasma proteins. These interactions cause opsonization and removal of nanoparticles by the immune system, and ultimately reduce the function of nanoparticles on the target cells.^{26,27} Therefore, the surface of MIONPs is coated with non-toxic and biocompatible compounds to improve the drug loading efficiency, stability, and performance in the target cell.^{28,29}

One of the most suitable candidates for coating is amino acids which are used to stabilize and modification of MIONPs.³⁰ Amino acids are inexpensive, non-toxic, and biocompatible.³¹⁻³⁴ Amino acids play important roles in the body. They can reduce tumor cells.^{35,36} It seems that amino acids could be exerted anti-cancer effects through

the activation of autophagy and apoptosis by inhibition of proteasome activity.³⁷

There are different reports on the synthesis of coated MIONPs with amino acids. In some studies, they have been loaded on various chemotherapy drugs.³⁸⁻⁴⁰ Lysine amino acid is one of the desirable biological molecules for coating magnetic nanoparticles.⁴¹ These carriers can prevent drug destruction and damage to healthy tissues.⁴²

In this study, TMX-loaded L-lysine coated MIONPs were synthesized and their potential toxicity was evaluated against MCF-7 BC cells.

Materials and Methods

Synthesis of F-Lys-TMX NPs

First, the magnetic iron oxide NPs stabilized by L-lysine, were synthesized in one step co-precipitation method. The aqueous solution (150 mL in deionized water) was prepared by dissolving 1.12 g $\text{FeCl}_3 \cdot 6\text{H}_2\text{O}$ and 0.45 g FeCl_2 (Merk, Darmstadt, Germany) (molar ratio 2:1, respectively) and stirred vigorously (12 000 rpm) under N_2 atmosphere at 60°C for 17 minutes. Then 1.65 g of L-lysine was added and stirred for 20 min at 60°C (changing the mixture color from yellow to brown indicates the formation of an iron complex with L-lysine). After that, 21 mL of NH_4OH (25%) was added to the mixture dropwise at a uniform rate in the presence of N_2 gas to increase the pH of the solution (pH ~11) and make the alkaline environment (ammonium hydroxide acts as a reducing agent). The reaction mixture was stirred for 6 hour (temperature 60°C and presence of N_2 gas) and a black suspension of Fe_3O_4 was formed. The prepared nanoparticles were magnetically separated using the external magnet (1.2 Tesla) for 6 minutes, and then were washed 3 times with deionized water. It was placed in the oven for 24 hours at 50°C to completely dry.⁴³ Additionally, the number of NPs obtained was 1.47 g.

To load TMX on the surface of L-lysine coated Fe_3O_4 magnetic nanoparticles (F-Lys NPs), 10 mg of F-Lys NPs was added to 2.8 mL of distilled water and stirred at 400 rpm. Then, 2.5 mg of TMX was dissolved in 2 mL of ethanol and added dropwise to the F-Lys NPs suspension, and stirred for 24 hours in darkness at room temperature. TMX is physically loaded on the surface of MIONPs and also it can also give a hydrogen bond with the amino acid lysine. TMX loaded nano-carriers (F-Lys-TMX NPs), were separated by the external magnet (1.2 Tesla) for 10 min and washed 3 times with deionized water, and then dried at room temperature.

Characterization of the F-Lys-TMX NPs

The chemical features of the F-Lys-TMX NPs were recorded by Fourier-transform infrared (FT-IR) spectroscopy (Bruker Tensor 27, Biotage, Germany). The FT-IR spectra were scanned between 4000 and 400 cm^{-1} at a resolution of 4 cm^{-1} in the transmittance mode.

The size and morphology of the F-Lys-TMX NPs were determined by transmission electron microscopy (TEM)

(Cambridge 360–1990 Stereo Scan Instrument-EDS) and scanning electron microscopy (SEM) (TESCAN MIRA3). Crystallographic structures of the F-Lys-TMX NPs were determined by a Bruker AXS model D8 Advance using Cu K α radiation in the range of $2\theta = 10^\circ - 90^\circ$.

The Zeta Potential of F-Lys-TMX NPs was determined by the dynamic light scattering method (DLS) (Malvern Instruments, Worcestershire, UK, Nano ZS). DLS analysis was carried out to evaluate the polydispersity index (PDI) and hydrodynamic size distribution (Malvern model 3600 Zetasizer (UK).

The thermal stability assay, vibrating sample magnetometer (VSM), and differential scanning calorimetry (DSC) analysis were performed according to the previous study.⁴³

Determination of loading efficiency

After drying the nanoparticles, it was weighed 3 times and each time 2 mg of the sample was dissolved in 10 mL of ethanol and placed on a shaker incubator at 37°C for 24 hours to release the loaded drug. The samples were then placed on a magnet to separate the nanoparticulate upper solution from the magnetic NPs. The absorbance of the upper solution was then measured by a spectrophotometer at 278 nm. Using the TMX calibration curve, the amount of loaded drug was calculated using the following equation:

$$\text{Drug loading content} = \frac{\text{weight of drug in nanocarrier}}{\text{weight of nanocarrier}} \times 100$$

Study of drug release

To study the in vitro drug release at pH 5.8 and pH 7.4, 1 mL of a buffer including 5 mg of the NPs was inserted into the dialysis bag (cut off 12 000 Da). It was immersed inside two containers containing 10 mL phosphate buffer (1M) pH 5.8 and 10 mL phosphate buffer pH 7.4, respectively. The contents were placed in a shaker incubator (50 rpm) at 37°C. At certain times, 2 mL of the outer solution of the dialysis bag was replaced with 2 mL of fresh buffer, and the amount of drug released was measured by the UV spectrophotometer at 278 nm. Each measurement was done twice and the average of these two data was used to compute the concentration of a free drug. The measured results were plotted as the amount of cumulative released drug according to the following equation for a period of 150 hours.

$$\text{Cumulative amount released (\%)} = \left(\sum_{t=0}^{t=t} \frac{M_t}{M_0} \right) \times 100$$

In the above equation, $\sum_{t=0}^{t=t} M_t$ is the amount of cumulative released drug of NPs in the time t , and m is the total amount of drug present in the NPs.

In vitro cytotoxicity assay and anticancer activity

Cell culture and MTT assay

The MCF-7 human breast cancer cell line (IBRC C10682),

was purchased from the Iranian Biological Resource Center (IBRC C10097). Briefly, 1×10^4 cell/well were seeded into 96-well plates followed by incubation overnight in a CO₂ incubator at 37°C. Then, the cells were treated with different concentrations of TMX, F-Lys NPs, and F-Lys-TMX NPs (1.7, 3.125, 7.5, 15, 20, 60, 125 $\mu\text{g/mL}$) for 24, 48 and 72 hours. In order to determine the cytotoxicity of TMX, F-Lys NPs, and F-Lys-TMX NPs against MCF-7 cells, the MTT method [3-[4,5-dimethylthiazol-2-yl]-2,5-diphenyltetrazolium bromide] was used. Then, the MTT was added into the wells and a plate was kept at 37°C in a 5% CO₂ for 4 hours. The MTT dye was removed and the formazan crystals were dissolved in dimethyl sulfoxide (DMSO). Finally, the absorbance was recorded at 570 nm using an ELISA Reader (Oraganon Teknika, Netherlands) and cell viability was determined. According to these results, IC₅₀ values and cell viability percentage were reported.⁴⁴

Apoptosis/necrosis assay and cell cycle analysis

The detection of apoptosis/necrosis ratio in MCF-7 cancer cells was carried out using Annexin V-FITC kit (Roch, Germany) according to the manufacturer's protocol. A flow cytometry device (Bio compare, USA) was used for cellular analysis. The MCF-7 cells (1×10^5 cell/well) were treated with IC₅₀ concentrations of F-Lys-TMX NPs, TMX, and F-Lys NPs for 24, 48, and 72 hours. The untreated MCF-7 cells were used as the control group.

For cell cycle assay, the MCF-7 cells were seeded into 6-well plates (1×10^6 cell/well) and incubated for 24 hours. Then, the semi-confluent cells were treated with IC₅₀ concentration of F-Lys-TMX NPs, TMX, and F-Lys NPs for 24, 48, and 72 hours. Following the treatment, the cancer cells were washed twice with PBS and harvested by centrifuging at 1500 rpm for 5 minutes. Subsequently, cell pellets were suspended in 250 μL of propidium iodide (PI) staining solution and kept at room temperature for 30 minutes. The profile of the cell cycle was detected using a BD FACScan Cell Flow Cytometer (Becton Dickinson, USA). The data were analyzed by Flow Jo software and reported as the percentage of the cell cycle.

Gene expression analysis

The MCF-7 cells were incubated with IC₅₀ concentrations of F-Lys-TMX NPs, TMX, and F-Lys NPs for 24, 48, and 72 hours. Then, RNA extraction and cDNA synthesis were carried out according to CinnaGen and RevertAidTM First Strand cDNA Synthesis Kit protocol (Fermentas, Burlington, Canada), respectively. The expression levels of β -actin (housekeeping gene), ERBB2, caspase-3, caspase-9, cyclin D1, and cyclin E genes were determined according to the SYBER Green method. A detail of Real-time PCR reaction and the thermal program have been described in our previous study.⁴⁵ The primers sequences are provided in Table 1.

Statistical analysis

The one-way ANOVA method was used for the statistical

Table 1. Primers sequences of target genes

Genes	Primers Sequences
<i>b-actin</i>	Forward: 5'-TCCTCCTGAGCGCAAGTAC-3' Revers: 5'-CCTGCTTGCTGATCCACATCT-3'
<i>Caspase 3</i>	Forward: 5'-CATACTCCACAGCACCTGGTTA-3' Revers: 5'-ACTCAAATTCTGTTGCCACCTT-3'
<i>Caspase 9</i>	Forward: 5'-CATATGATCGAGGACATCCAG-3' Revers: 5'-TTAGTTCGCAGAAACGAAGC-3'
<i>Cyclin D1</i>	Forward: 5'-CAGATCATCCGCAAACACGC-3' Revers: 5'-AAGTTGTTGGGGCTCCTCAG-3'
<i>Cyclin E</i>	Forward: 5'-CTCCAGGAAGAGGAAGGCAA-3' Revers: 5'-TTGGGTAAACCCGGTCATCA-3'
<i>ERBB2</i>	Forward: 5'-TTCCTAAGGCTTTCAGTACC-3' Revers: 5'-GAGTCTTTGTGGATTCTGAGG-3'

analysis by SPSS version 19.0 software (SPSS Inc., Chicago, IL, USA). The expression levels of genes were analyzed by Tukey's HSD post hoc test. The results were expressed as mean \pm standard deviation (SD) of three replicates and P value < 0.05 was considered as significant.

Results

Characterization of the F-Lys-TMX NPs

The FTIR spectra of bare Fe_3O_4 , F-Lys NPs, F-Lys-TMX NPs, and free TMX were shown in Fig. 1. The presence of L-lysine coating on Fe_3O_4 NPs was clearly obvious from the comparison of the FT-IR spectrum of bare Fe_3O_4 with Fe_3O_4 coated with pure L-lysine. The bare Fe_3O_4 has distinct peaks in the 610 cm^{-1} and 444 cm^{-1} which are related to Fe-O vibration.⁴⁶

The F-Lys NPs spectrum indicates the absorption peaks related to bare Fe_3O_4 and the carbonyl group of the L-lysine. For F-Lys NPs, the peaks at ~ 1388 , 1628 , 2922 , and 3428 cm^{-1} related to C-O and C=O stretching vibrations, C-H stretching of methylene groups, N-H stretching vibration overlap with OH stretching, respectively. The peaks of 1507 cm^{-1} and 1477 cm^{-1} (C=C ring stretching), 3027 cm^{-1}

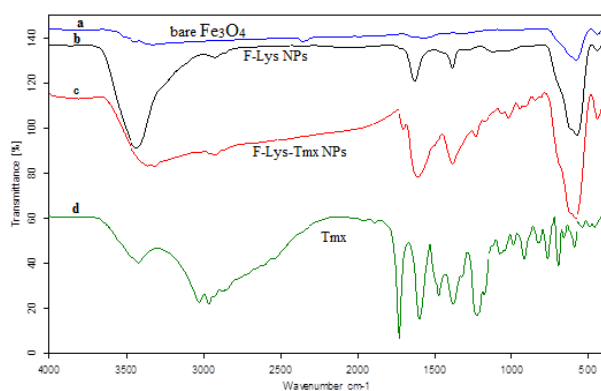


Fig. 1. FT-IR spectra of bare Fe_3O_4 (a), F-Lys NPs (b), F-Lys-TMX NPs (c), and free TMX (d). F: Fe_3O_4 magnetic nanoparticles; F-Lys NPs: L-lysine coated magnetic Fe_3O_4 nanoparticles; F-Lys-TMX NPs: Tamoxifen-loaded L-lysine coated magnetic Fe_3O_4 nanoparticles; TMX: Tamoxifen.

(= C-H stretching), 3180 cm^{-1} (-NH₂) are related to the FT-IR spectrum of TMX.

The FT-IR spectrum of F-Lys-TMX NPs indicates the peaks of TMX in 1724 cm^{-1} resulting from the ketonic group, 1588 cm^{-1} from amine (N-H bend) and 1384 cm^{-1} from the methyl group and the peaks related to Fe_3O_4 are strong peaks at 613 and 444 cm^{-1} , which indicates Fe-O vibration.⁴³

The TEM and SEM micrographs to investigate the size and morphology of the synthesized F-Lys-TMX NPs are presented in Fig. 2A-B. The F-Lys-TMX NPs had spherical in shape with a size ranging from 9 to 30 nm.

The XRD pattern of F-Lys-TMX NPs is presented in Fig. 3. The position and relative intensity of all characteristic diffraction peaks of the F-Lys-TMX NPs were closely matched with the pattern of the standard Fe_3O_4 NPs demonstrating the successful synthesis of the NPs. The peaks in F-Lys-TMX NPs spectrum are at 2θ equals 18.49° , 30.38° , 35.74° , 43.82° , 54.71° , 57.53° , and 63.24° corresponding to planes of (111), (220), (311), (400), (422), (511), and (440), respectively.³⁹

The presence of L-lysine and TMX at the surface of the magnetic nanoparticles was confirmed by changes in the Zeta potential. The Zeta potential of bare Fe_3O_4 was about -5.83 mV , after coating the surface of the NPs with L-lysine, the Zeta potential of F-Lys NPs was changed to 2.98 mV . After loading TMX, the ζ -potential of F-Lys-TMX NPs was reduced to -7.58 mV (Fig. 4A).

The average size of the NPs was determined by DLS method at 153.7 nm and PDI was 0.1. The PDI value indicates the monodispersity of the NPs (Fig. 4B).

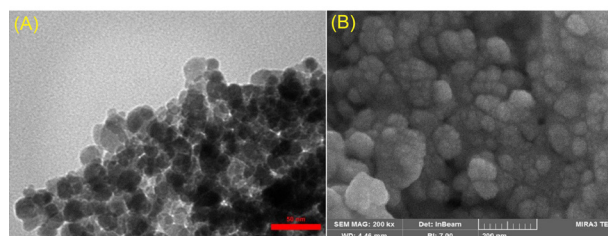


Fig. 2. TEM (A) and SEM (B) micrographs of F-Lys-TMX NPs.

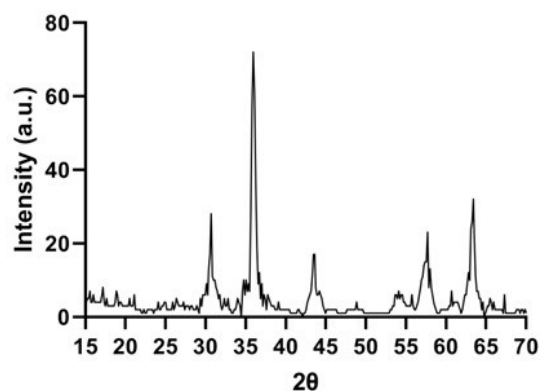


Fig. 3. XRD Pattern of F-Lys-TMX NPs.

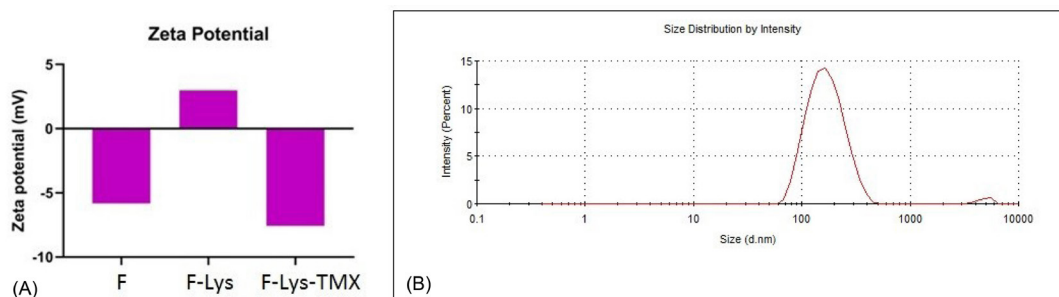


Fig. 4. ζ -potential of bare Fe₃O₄, F-Lys NPs and F-Lys-TMX NPs (A). DLS analysis of F-Lys-TMX NPs (B).

The thermogravimetric analysis (TGA) curves of the F-Lys NPs and F-Lys-TMX NPs are presented in Fig. 5. About 5.2% weight loss was observed after heating F-Lys NPs to 500°C. After TMX loading, a much higher weight loss (about 18.3%) was observed in the F-Lys-TMX NPs, which is consistent with the increase in organic content of the NPs upon loading of TMX.

Supportive evidence for the F-Lys-TMX NPs can also be provided by DSC. Fig. 6 shows thermograms of F-Lys NPs, free TMX, and F-Lys-TMX NPs. A melting point of L-lysine shifted to a lower temperature after coating on bare Fe₃O₄ NPs surface indicates the coating of IONPs with L-lysine. The melting points of F-Lys NPs and TMX were detected at 201.61°C and 146.15°C, respectively, and a single endothermic peak at 305.82°C was detected in DSC thermogram of F-Lys-TMX NPs. However, any peak visible near the F-Lys NPs and TMX melting point in the F-Lys-TMX NPs thermogram was appeared, which approves the loading of TMX and the absence of any unloading TMX in the synthesized nanoparticles.

VSM of F-Lys-TMX NPs for detection of the magnetic properties of the synthesized NPs provide evidence that F-Lys-TMX NPs were superparamagnetic at room temperature. The saturation magnetization (MS) of the bare Fe₃O₄ was determined to be 76.29 emu/g. Modification of the magnetic NPs surface by L-lysine, and TMX decreased MS to 47.83 emu/g. The MS decrement

for F-Lys-TMX NPs can be clarified by the coating of L-lysine and the loading of TMX on the magnetic NPs (Fig. 7).

Drug release

The drug loading ratio of TMX in F-Lys-TMX NPs was 2.80%0.2. The drug release was examined at pH 5.8 and pH 7.4. As controls, the release of free TMX was studied to verify that the dispersion of drug molecules through the dialysis membrane was not a rate-limiting step during the release procedure. The results of the drug release graph in Fig. 8 showed that free TMX was released rapidly and reached its peak of 83% of the total in the first 20 hours at pH 7.4. About 25% of the drug from the drug-loaded nanoparticles was released at both pH values in the first few hours (about 12 hours). At pH 7.4 after 70 hours about 50% of the drug was released and after 120 hours the drug release was stable. However, at pH 5.8, about 75% of the drug was released and after 95 and 100 hours, the drug release was stable. Because in acidic conditions, H absorbed by NH₂ groups of TMX and L-lysine, leads to increased drug release.

Cell viability

The cytotoxicity effects of F-Lys-TMX NPs against MCF-7 cancer cells revealed that synthesized NPs significantly inhibited the proliferation of BC cells. The

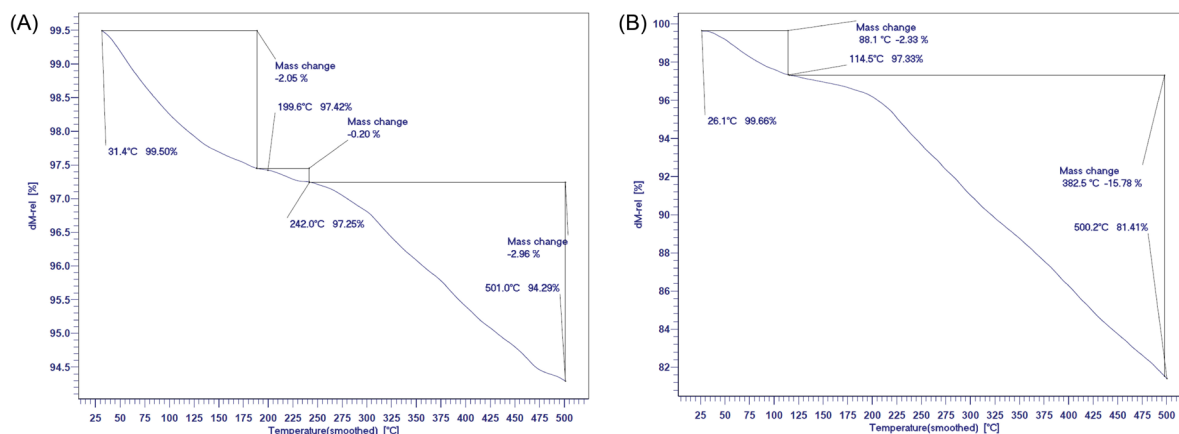


Fig. 5. TGA curves of F-Lys NPs (A) and F-Lys-TMX NPs (B).

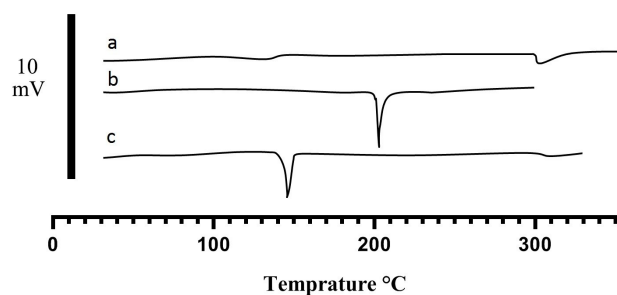


Fig. 6. DSC thermograms of F-Lys-TMX NPs (a), F-Lys NPs (b), and free TMX (c).

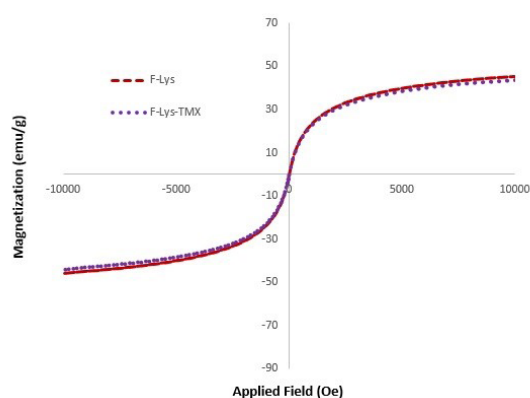


Fig. 7. VSM curves of F-Lys-TMX NPs and F-Lys NPs.

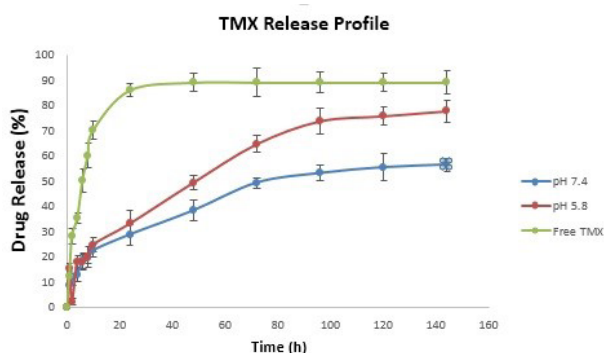


Fig. 8. The release profile of F-Lys-TMX NPs at pH 7.4 and 5.8 compared to free TMX.

anti-proliferative activity was time- and dose-dependent manner.

The IC_{50} value of the synthesized NPs was 11.3, 3.32, and 1.37 $\mu\text{g}/\text{mL}$ after 24, 48, and 72 hours, respectively indicating that the concentration of IC_{50} decreased with increasing the treatment time. According to the results, cell viability was reduced by increasing the treatment time and concentration of free TMX. The IC_{50} values of TMX in MCF-7 were calculated 4.4, 3.4, and 1.9 $\mu\text{g}/\text{mL}$ for 24, 48, and 72 hours, respectively.

The MTT assay indicated that F-Lys NPs had a very low cytotoxic effect on MCF-7 cells. The IC_{50} concentrations

of F-Lys NPs in MCF-7 cancer cells after 24, 48, and 72 hours were 563.37, 531.32, and 471.3 $\mu\text{g}/\text{mL}$, respectively (Fig. 9).

Apoptosis/necrosis detection

The induction of apoptosis was detected in the cells after treatment with F-Lys-TMX NPs at all times (Fig. 10). Following 24, 48, and 72 hours, 19.82%, 53.10%, 58.6% apoptosis were observed, respectively. After 24 hours of treatment with free TMX, 8.75% of the cells showed apoptosis. Following 48 and 72 hours, 36.1% and 45.7% apoptosis were detected, respectively. The results revealed that with increasing the treatment time with the synthesized nanoparticles and free TMX, more apoptosis was observed in the cells. Also, less apoptosis was detected in F-Lys NPs treated cells compared to F-Lys-TMX NPs and free TMX. So that, after 24, 48, 72 hours, 6.63%, 17.79%, and 21.85% apoptosis was seen, respectively. Totally, the study of apoptosis by flow cytometry confirmed higher apoptosis induction by F-Lys-TMX NPs compared to the free TMX and F-Lys NPs.

Cell cycle arrest

Following treatment of MCF-7 cells with F-Lys-TMX NPs and free TMX, the accumulation of MCF-7 cells in the G₀/G₁ phase was observed (Fig. 11). F-Lys-TMX NPs exhibited increased percentage of cell population of sub-G₁ phase (14.94%, 40.53%, 54.04% for 24, 48, and 72 hours, respectively) in comparison with free TMX (9.9%, 33.57%, 44.93% for 24, 48, and 72 hours, respectively). But no significant changes were detected after treatment of MCF-7 with F-Lys NPs in comparison with control cells (untreated MCF-7 cells). The results showed that, with increasing the treatment time by F-Lys-TMX NPs and free TMX, the percentage of sub-G₁ cell population increased and the percentage of G₁ and S stages cell population decreased.

Gene expression levels

In the cancer cells treated with F-Lys-TMX NPs, a significant up-regulation of Caspase-3 and -9 genes expression levels was observed with increasing the treatment time ($P < 0.05$). The expression levels of the cyclin D1, cyclin E, and ERBB2 genes were down-regulated. This down-regulation was significant at 48 and 72 hours for all three genes compared to the control group ($P < 0.05$) (Fig. 12).

A significant increase was also observed in Caspase-3 gene expression in free TMX-treated cells for 24, 48, and 72 hours ($P < 0.05$). An increase in the expression of caspase-9 after 48 and 72 hours of TMX treatment was significant ($P < 0.05$). By increasing the treatment duration, the expression levels of caspase-3 and -9 genes increased while the expression levels of cyclin D1, cyclin E, and ERBB2 genes decreased so that the lower expression of all these three genes in 48 and 72 hours was significant

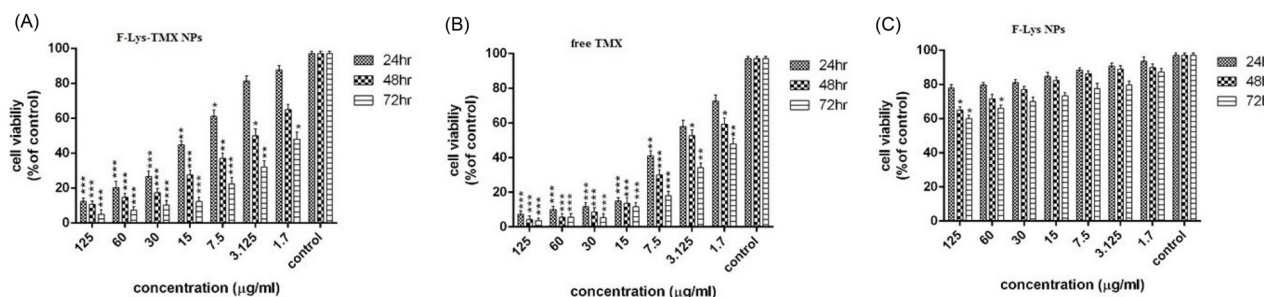


Fig. 9. The Cell viability of MCF-7 cells following incubation with F-Lys-TMX NPs (A), free TMX (B), and F-Lys NPs (C) for 24, 48, and 72 h (results are reported as viability in comparison with control cells [*** $P \leq 0.001$, ** $P \leq 0.01$, * $P \leq 0.05$] ($n = 3$). Control cells: untreated MCF-7 cells.

in comparison with the control group.

No significant changes were observed in the gene expression levels after treatment of MCF-7 cells with F-Lys NPs. There was no significant increase in the expression levels of the Caspase-9 gene after treatment in three-time points than the control group ($P > 0.05$). Also, no significant reduction was detected in the expression levels of cyclin D1, cyclin E, and ERBB2. There was also no significant increase in the caspase-3 gene expression levels for 24 and 48 hours ($P > 0.05$). Only after 72 hours of treatment with F-Lys NPs, a significant increase was

detected ($P < 0.05$).

Discussion

The anti-estrogen molecule, TMX, is a strong and hydrophobic hormone drug that is widely used to treat BC in patients at high risk.^{47,48} TMX is a selective estrogen receptor modulator that is used to treat hormone-responsive cancers and prevents androgen receptor activation as an antagonist.⁴⁹

Most anti-cancer drugs have lethal effects on the cells. These effects are not limited to the cancer cells in most

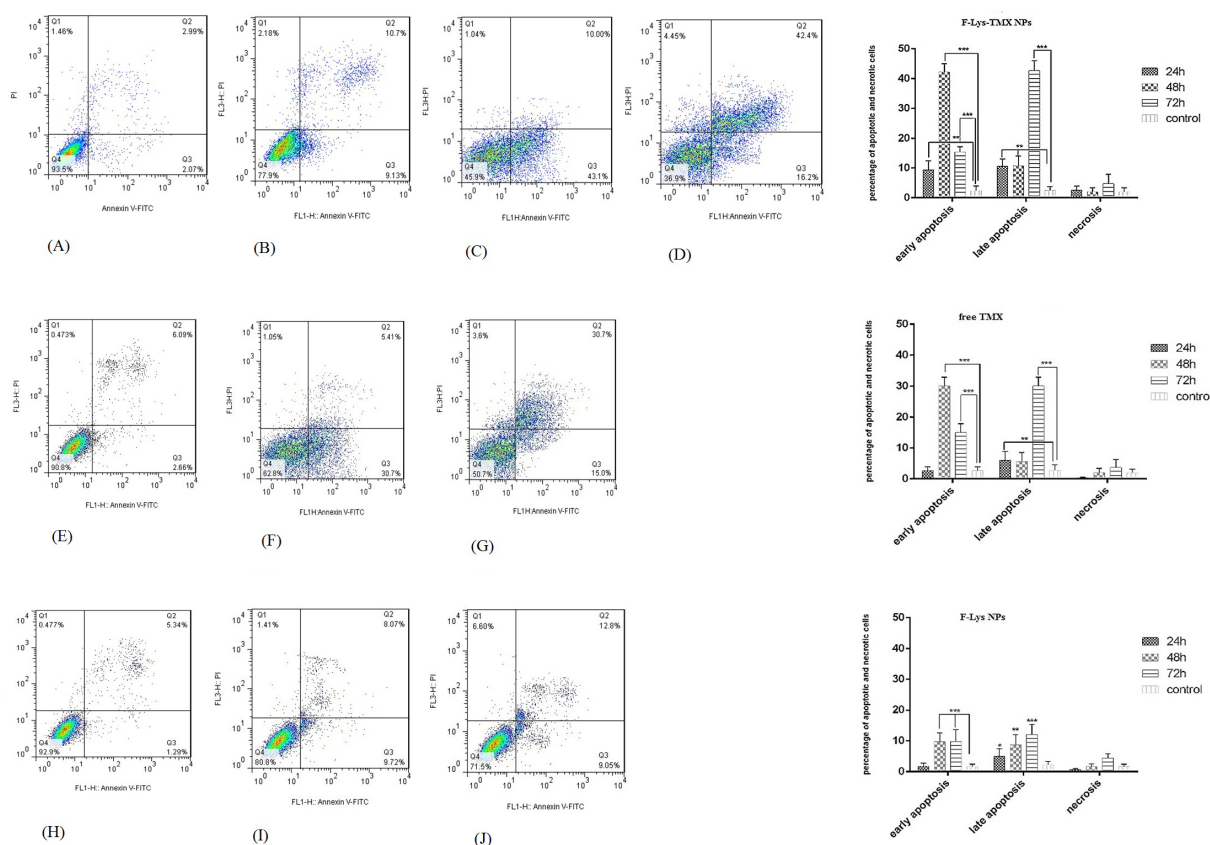


Fig. 10. Flow cytometry plots for evaluating apoptosis in control cells (A) and MCF-7 cells treated with IC50 concentrations of F-Lys-TMX NPs (B-D), free TMX (E-G), and F-Lys NPs (H-J) for 24, 48, and 72 h. The mean (\pm standard deviation, SD) of the three independent experiments of early apoptosis, late apoptosis, necrosis, and viable cells are reported in MCF-7 cells incubated with F-Lys-TMX NPs, free TMX, and F-Lys NPs in comparison with control group [*** $P \leq 0.001$, ** $P \leq 0.01$, * $P \leq 0.05$]. *control cells: untreated MCF-7 cells. Q3 represents early apoptotic cells with Annexin-FITC + and PI⁻ staining index, Q2 represents late apoptotic cells with Annexin-FITC + and PI +, Q3 represents healthy cells with Annexin-FITC⁻ and PI⁻ staining index and Q1 is necrotic cells with Annexin-FITC⁻ and PI + staining index.

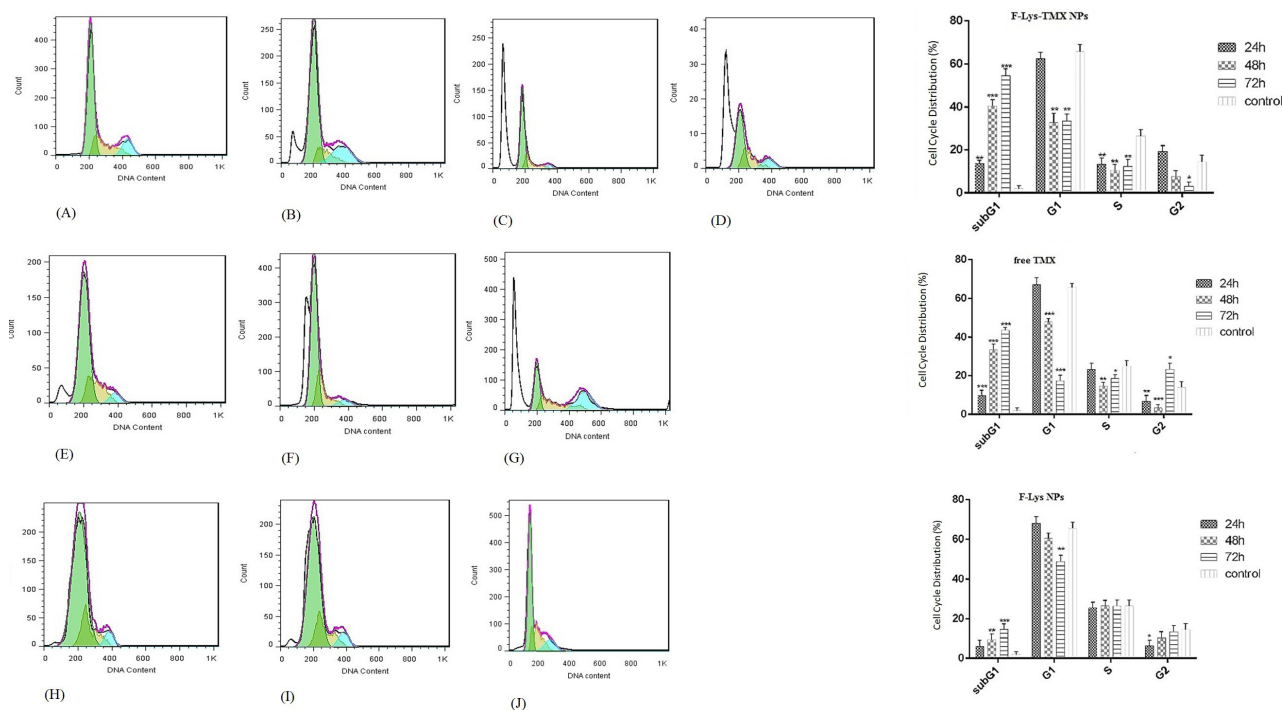


Fig 11. Cell cycle arrest analysis in control cells (a) and MCF-7 cells treated with IC50 concentrations of F-Lys-TMX NPs (B-D), free TMX (E-G), and F-Lys NPs (H-J) for 24, 48, and 72 h. The mean (\pm standard deviation, SD) of the three independent experiments of sub G1, G1, S, and G2 cell cycle phase are reported in MCF-7 cells incubated with F-Lys-TMX NPs, free TMX, and F-Lys NPs in comparison with control group [*** $P \leq 0.001$, ** $P \leq 0.01$, * $P \leq 0.05$]. *Control Cells: untreated MCF-7 cells.

cases but include the healthy cells as well. Drug delivery systems have been designed through nanotechnology to reduce the side effects of chemotherapy drugs as well as reduction of its dosage. Also, drug delivery systems have significantly improved the pharmacological treatments due to drug pharmacokinetic changes, increased drug bioavailability in the bloodstream, decreased toxicity, and increased half-life of the drug.^{50,51}

In addition to the general characteristics of nanoparticles including their biocompatibility for use in clinical cases, and very high level of surface-to-volume ratio in these compounds, the capacity of their loading by drugs or the compounds used in gene therapy is heavily increased. Nanoparticles with hundreds or thousands of times smaller size than human cells can make a lot of interactions at the intracellular level and can provide several benefits in the diagnosis and treatment of cancers.⁵²

Magnetic NPs have facilitated a wide range of diagnostic and therapeutic applications in diseases including cancer. Magnetic and superparamagnetic NPs are used as effective nanocarriers in chemotherapy drugs transfer due to special properties such as being non-invasive and high targeting efficiency.⁵³

Studies conducted over the recent years on MIONPs show that these particles have no quick or prolonged toxic effects on the body. However, the presence of some NPs together with nanocarriers enhances their effect and function on cancer cells. These NPs reinforce the effects

of nanocarriers by various mechanisms such as increased oxidative stress and proper accumulation of the drug in the cell.⁵⁴

The co-precipitation method is the simplest and the most efficient chemical method for the synthesis of magnetic nanoparticles. The main advantage of co-precipitation is the ability to synthesize a large number of NPs.⁴³

In this study, the surface of the magnetic iron oxide NPs was coated by L-lysine amino acid for stability. The advantage of using L-lysine as a coating agent is that it can be used in the body. It is involved in calcium absorption, bone development, and collagen production. It is also involved in the production of antibodies and is used by different enzymes and hormones. It is also needed to repair tissues.³⁹

The synthesized NPs in the present study had an appropriate size and surface charge. Since the plasma and blood cells have a negative charge surface, the NPs with a slight negative charge can decrease the nonspecific interactions with these compounds by electrostatic interactions.⁵⁵

The difference observed in the size of NPs is due to the different sensitivities of different methods. The size of NPs measured with DLS is larger than what was measured by SEM or TEM.³⁹

Zeta potential is an important factor for evaluating the stability of NPs. According to the zeta potential value, the F-Lys-TMX NPs exhibited a good stability.⁵⁶

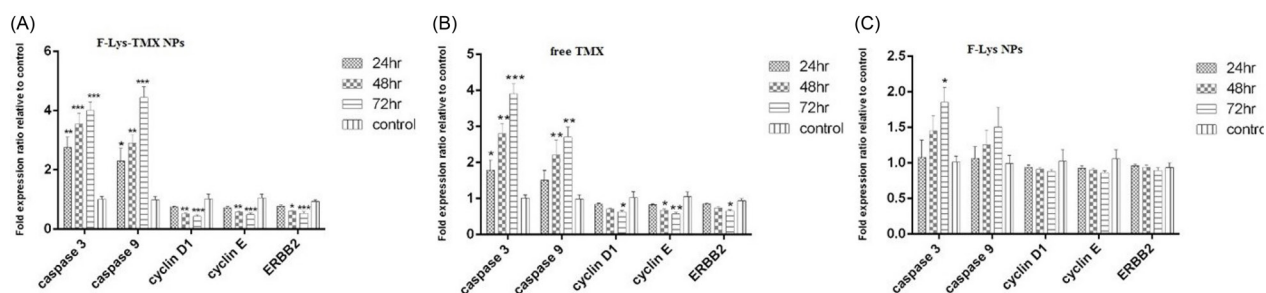


Fig. 12. Expression levels of Caspase 3 and Caspase 9, Cyclin D1, Cyclin E, and ERBB2 genes following treatment of MCF-7 cells with F-Lys-TMX NPs (a), free TMX (b), and F-Lys NPs (c) for 24, 48, and 72 h. The results are reported as delta cycle threshold and fold change of gene expression compared to control cells [*** $P \leq 0.001$, ** $P \leq 0.01$, * $P \leq 0.05$] ($n = 3$). *Control Cells: untreated MCF-7 cells.

The size of the NPs is an important parameter in targeted drug delivery. Few studies have shown that particles smaller than 1 μm undergo uniform capillary distribution.⁵⁷ In most solid tumors vascular permeability is high. The particles smaller than 400 nm can pass by the vascular endothelial network and accumulate in tumor sites through the enhanced permeability and retention effect.^{58,59}

The particles' hydrodynamic size plays an important role in hiding them from the phagocytic system of the body. The larger NPs are easily trapped by the liver, while smaller particles that are more useful for medical applications are later detected by the liver. This causes a longer half-life in the bloodstream.⁶⁰

The effects of F-Lys-TMX NPs and free TMX, as well as F-Lys NPs alone, were compared in the MCF-7 BC cell line.

The study of the cytotoxic effects of F-Lys NPs, TMX, and the F-Lys-TMX NPs showed that F-Lys NPs alone were not able to inhibit the proliferation of MCF-7 cells, but the synthesized NP loaded with TMX had high efficacy to prevent the proliferation of MCF-7 cancer cells. The results also showed that the inhibitory process of cell proliferation follows a time- and dose-dependent manner. The potency and efficiency of the synthesized F-Lys-TMX NPs in inhibiting the cancer cells' growth were comparable and even more powerful than TMX. It was confirmed by comparing drug IC_{50} value, cell apoptosis, cell cycle analysis, and the expression pattern of the genes involved in cell proliferation.

The IC_{50} value of the F-Lys-TMX NPs after 48 and 72 hours was 3.23 and 1.37 $\mu\text{g}/\text{mL}$, respectively and for TMX was 3.4 and 1.9 $\mu\text{g}/\text{mL}$, respectively. It was shown that F-Lys-TMX NPs at a lower concentration than TMX could inhibit the proliferation of MCF-7 cells.

In this regard, the results showed that synthesized F-Lys-TMX NPs were able to induce apoptosis significantly in MCF-7 cells in comparison with TMX and also F-Lys NPs alone. The induced apoptosis in the cells treated with F-Lys-TMX NPs For 48 and 72 hours (53.1% and 58.6%, respectively) were significantly higher than those treated with free TMX for 48 and 72 hours (36.1% and 45.7%,

respectively).

The drug release at pH 7.4 is much slower than pH 5.8, which is of great importance. Faster release of the drug at acidic pH can occur due to protonation of the drug. As the pH of cancer cells is acidic and the pH of the bloodstream is 7.4, the nano-drug must be highly stable in the bloodstream and during circulation to retain the drug until it is delivered to the target tissue. This feature lessens drug side effects. On the other hand, when nanoparticles are absorbed by the tumor cells by the endocytosis process, it may have a better chance of releasing the drug around the tumor sites or inside endosomes or lysosomes of tumor cells at acidic pH, which is an important process in the targeted treatment of cancers.⁶¹⁻⁶³

TMX-loaded magnetic NPs are more toxic than free TMX in cancer cells. Chitosan-polyvinylpyrrolidone-bovine serum albumin-coated magnetic iron oxide (Fe_3O_4 -CS-PVP-BSA) nanoparticles with the size range between 300 to 600 nm and positive zeta potential had a higher apoptotic induction power than free TMX. Their encapsulation efficiency was between 63% and 96%.⁶⁴

Also, TMX-loaded magnetite/PLLA composite NPs with an average size of 200 nm had higher cell toxicity effects against MCF-7 cancer cells than TMX. The encapsulation efficiency was between 60% and 80% for TMX.⁶⁵

The average size of Fe_3O_4 -APS-PEG nanoparticles synthesized by Majd et al was 40 nm. The loading efficiency was 49.1% and drug release in 24 and 48 hours was 80% and 90%, respectively. The apoptosis induced by Fe_3O_4 -APS-PEG-FA-TMX NPs in MCF7 cells was reported to be greater than 95%.⁶⁶

In a study by Nosrati et al, TMX was loaded onto the magnetic NPs of tyrosine-coated iron oxide and synthesized nano-drug in the size of 19.22 nm. Its cytotoxic study on MCF-7 cells revealed that by increasing the time and concentration, the synthesized nano-drug was more toxic than that of free TMX. The magnetic nanoparticles of tyrosine-coated iron oxide alone had no cytotoxicity on the cells, similar to those observed in the present study.⁴³ The results of drug release in their study showed that drug release at pH 7.4 and pH 5.5 was 40% and 70%, respectively, which is comparable to our research results

(50% at pH 7.4 and 65% at pH 5.5), so that drug release in F-Lys-TMX NPs at pH 7.4 was 10% higher than F-Tys-TMX NPs.

To eliminate drug therapy constraints in cancer therapy, a polymeric nanocomposite containing TMX was synthesized with a size of about 49.89 nm by Akim and colleagues. Its cytotoxicity effect on MCF-7 cells showed that the synthesized nano-drug was more toxic than TMX only at 48 and 72 hours, and the polymerized nanoparticle alone did not have any cytotoxic effects on the cells.⁶⁷

The higher apoptosis activity of TMX-loaded NPs compared to free TMX appears to be due to the accumulation and better absorption of nanoparticles in tumor cells.^{64,68}

The negative surface charge of the nanoparticles prevents the aggregation of the nanoparticles. Particles with small sizes have a higher accumulation rate and penetration power into the cell.⁶⁹

Due to the low solubility of TMX alone and its high affinity for the plasma proteins in the growth medium, it appears to be less effective than TMX-loaded nanoparticles. On the other hand, by absorbing nano-carriers by MCF7 cells, TMX is released directly into the cells. Its increase in intracellular concentration increases its anti-cancer activity.^{65,70}

Similar to our study, unloaded magnetic nano-carriers, including Fe₃O₄-CS-PVP-BSA, Fe₃O₄-APS-PEG, unloaded magnetite/PLLA, and Hollow IONPs did not have significant toxicity to MCF-7 cells.^{62,64-66}

The expression levels of the Cyclin D1 and Cyclin E genes were down-regulated after treatment with F-Lys-TMX NPs and free TMX. This expression reduction in MCF-7 cells treated with F-Lys-TMX NPs was higher than those treated with TMX. As a result, following down-regulation of Cyclin D1 expression levels, the cells were arrested at the G0/G1 phase. By increasing time, the percentage of sub-G1 cells increased and the cell cycle progress and entrance to the next phase were prevented. As mentioned before, the Cyclin D1 directs the G1 phase progress.

The results of the cell cycle assay were consistent with the results of the expression pattern of the genes involved in promoting the cell cycle, induction of apoptosis, and cell proliferation. The reduced cyclin D1 and E expression and increased expression of genes involved in apoptosis (caspase-3 and -9), were more effective in the treatment with F-Lys-TMX NPs compared to the free TMX.

According to the results of the present study, the expression levels of the ERBB2 gene in MCF-7 cancer cells treated with F-Lys-TMX NPs and the cells treated with TMX decreased significantly. Down-regulation of expression levels of the ERBB2 gene was more obvious in the cells treated with the F-Lys-TMX NPs compared to the free TMX.

It should be noted that no significant changes were observed in the expression levels of genes and percentage of

the cell cycle after treatment with magnetic nanoparticles.

The mRNA level of the cyclin D protein increases in 50% of BCs. Cyclin D gene is a proto-oncogene. The oncogenes like epidermal growth factor receptor and estrogen both apply their mitogenic effects by activating the transcription of the cyclin D1 gene. In the promoter region of the cyclin D1 gene, there is no estrogen response element, thus, the estrogen receptor (ER) may act as an activating aid at the transcriptional level. In fact, cyclin D1 enhances the transcription of estrogen receptor-dependent, by binding to the hormone-binding domain in ER and the increase in proteins interactions activity with the help of ER activators.⁷¹

In general, TMX with more than one pathway can exert its cytotoxic properties. Among the ER-related pathways, TMX enhances the transformation of the growth factors β 1 and pleiotropic cytokines, which are the main regulators for the proliferation and functional activity of the cells. Besides, TMX can make a competitive binding with estrogen-dependent receptors and form the TMX-ER complex, which blocks the binding of estrogen to the receptor. The attachment of the TMX-ER complex to the estrogen responder which includes estrogen-sensitive genes reduces the transcription of these genes, blocks cell cycle in the G1 phase, reduces cell proliferation, and induces apoptosis.⁷²

TMX blocks the growth factors such as ERBB2/HER2. High levels of ERBB2 have been observed in TMX-resistant cancers.⁷³ TMX requires PAX2 protein for its anticancer effect. By increasing the expression of PAX2, the TMX-ER complex can suppress the expression of the pro-proliferative protein ERBB2.⁷⁴

Lipopolymeric NPs loaded with TMX, similar to our research were able to induce apoptosis in MCF-7 cells and arrest the cell cycle in the G0/G1 phase.⁷⁵ The apoptosis was evaluated in the cells after 12 and 24 hours, which resulted in more apoptosis in 24 hours. However, in the present study, after 48-hour treatment with F-Lys-TMX-NPs, significant apoptosis was observed in the cells. The comparison of the cell cycle analysis also showed that the synthesized F-Lys-TMX NPs in our study had more efficiency and potency in the cell cycle arrest in the G0/G1 phase and increasing the cell population in the sub-G1 phase compared to the synthesized nanocarrier.

In another study, the cytotoxic effect of TAM-loaded solid lipid nanoparticles (SLNs) in MCF-7 cells was evaluated approximately equal to TMX. The IC₅₀ value of their synthesized NPs was several times higher than that of F-Lys-TMX NPs in our research: (12.5 and 11.78 μ g/mL vs. 3.23 and 1.37 μ g/mL for 48 and 72 hours, respectively). Also, the cell cycle analysis showed that SLNs arrested the cell cycle at the G0/G1 phase which was similar to what was found in the present study.⁷⁶ It seems that the F-Lys-TMX NPs in our research have stronger performance than SLNs.

In the present study, several biological tests including the

Research Highlights

What is the current knowledge?

- ✓ Chemotherapy drugs including TMX, cause drug resistance in addition to many side effects.
- ✓ Due to the side effects of chemotherapy drugs, the development of nanoscience-based drug delivery systems has been developed.
- ✓ Magnetic nanoparticles are used as effective nano-carriers in chemotherapy drugs transfer due to their special properties.

What is new here?

- ✓ F-Lys-TMX NPs are more effective and have potential for the cell proliferation inhibition and apoptosis induction compared to the TMX.
- ✓ F-Lys-TMX NPs significantly inhibited the proliferation of MCF-7 BC cells in a dose-, and time-dependent manner.
- ✓ F-Lys-TMX NPs can be used as anticancer biological products for the treatment of BC, after further investigation.

expression levels of genes involved in cellular apoptosis and cell cycle analysis were performed to demonstrate the anti-cancer activity of F-Lys-TMX-NPs. The results showed that the F-Lys-TMX-NPs in this study had stronger anti-cancer activity and apoptosis induction compared to the TMX alone for MCF-7 cells.

Conclusion

The results of this study showed that loading TMX on lysine-coated magnetic IONPs makes a new nano-drug with greater efficacy and better efficiency than TMX alone in the treatment of BC. The synthesized F-Lys-TMX NPs showed stronger anti-proliferative properties and anti-cancer effects than that free TMX.

Acknowledgment

The authors would like to acknowledge the laboratory of Islamic Azad University.

Funding sources

There is no funding.

Ethical statement

Not applicable.

Competing interests

The authors declared no conflict of interest regarding the publication of this paper.

Authors' contribution

S.R. performed most of the experiments, methodology, and cell culture study. F.T. contributed to this study by designing the experimental plans, performing data analysis, supervision, writing - review & editing, and project administration. H.K. contributed to designing the experimental plan and data analysis in the synthesis of magnetic nanoparticles and characterization.

References

1. Ferlay J, Soerjomataram I, Dikshit R, Eser S, Mathers C, Rebelo M,

- et al. Cancer incidence and mortality worldwide: sources, methods and major patterns in GLOBOCAN 2012. *Int J Cancer* **2015**; 136: E359-86. <https://doi.org/10.1002/ijc.29210>
2. Nafissi N, Khayamzadeh M, Zeinali Z, Pazooki D, Hosseini M, Akbari ME. Epidemiology and histopathology of breast cancer in Iran versus other Middle Eastern countries. *MEJC* **2018**; 9: 243-51. <https://doi.org/10.30476/MEJC.2018.42130>
3. Zeichner SB, Ambros T, Zaravinos J, Montero AJ, Mahtani RL, Ahn ER, et al. Defining the survival benchmark for breast cancer patients with systemic relapse. *Breast Cancer (Auckl)* **2015**; 9: 9-17. <https://doi.org/10.4137/BCBCR.S23794>
4. An KC. Selective Estrogen Receptor Modulators. *Asian Spine J* **2016**; 10: 787-91. <https://doi.org/10.4184/asj.2016.10.4.787>
5. Mourits MJ, De Vries EG, Willemsse PH, Ten Hoor KA, Hollema H, Van der Zee AG. Tamoxifen treatment and gynecologic side effects: a review. *Obstet Gynecol* **2001**; 97: 855-66. [https://doi.org/10.1016/s0029-7844\(00\)01196-0](https://doi.org/10.1016/s0029-7844(00)01196-0)
6. Gill BL, Simpson JF, Somlo G, McGonigle KF, Wilczynski SP. Effects of tamoxifen on the cytology of the uterine cervix in breast cancer patients. *Diagn Cytopathol* **1998**; 19: 417-22. [https://doi.org/10.1002/\(sici\)1097-0339\(199812\)19:6<417::aid-dc3>3.0.co;2-p](https://doi.org/10.1002/(sici)1097-0339(199812)19:6<417::aid-dc3>3.0.co;2-p)
7. Szakács G, Paterson JK, Ludwig JA, Booth-Gentle C, Gottesman MM. Targeting multidrug resistance in cancer. *Nat Rev Drug Discov* **2006**; 5: 219-34. <https://doi.org/doi.org/10.1038/nrd1984>
8. Kirkin V, Joos S, Zornig M. The role of Bcl-2 family members in tumorigenesis. *Biochim Biophys Acta* **2004**; 1644: 229-49. <https://doi.org/10.1016/j.bbamcr.2003.08.009>
9. Kruh GD. Introduction to resistance to anticancer agents. *Oncogene* **2003**; 22: 7262-4. <https://doi.org/10.1038/sj.onc.1206932>
10. Calderwood SK, Khaleque MA, Sawyer DB, Ciocca DR. Heat shock proteins in cancer: chaperones of tumorigenesis. *Trends Biochem Sci* **2006**; 31: 164-72. <https://doi.org/10.1016/j.tibs.2006.01.006>
11. Memisoglu-Bilensoy E, Vural I, Bochoth A, Renoir JM, Duchene D, Hincal AA. Tamoxifen citrate loaded amphiphilic beta-cyclodextrin nanoparticles: in vitro characterization and cytotoxicity. *J Control Release* **2005**; 104: 489-96. <https://doi.org/10.1016/j.jconrel.2005.03.006>
12. Heidari Majd M, Asgari D, Barar J, Valizadeh H, Kafil V, Abadpour A, et al. Tamoxifen loaded folic acid armed PEGylated magnetic nanoparticles for targeted imaging and therapy of cancer. *Colloids Surf B Biointerfaces* **2013**; 106: 117-25. <https://doi.org/10.1016/j.colsurfb.2013.01.051>
13. Jabr-Milane LS, van Vlerken LE, Yadav S, Amiji MM. Multifunctional nanocarriers to overcome tumor drug resistance. *Cancer Treat Rev* **2008**; 34: 592-602. <https://doi.org/10.1016/j.ctrv.2008.04.003>
14. Fei L, Perrett S. Effect of nanoparticles on protein folding and fibrillogenesis. *Int J Mol Sci* **2009**; 10: 646-55. <https://doi.org/10.3390/ijms10020646>
15. Moore A, Basilion JP, Chiocca EA, Weissleder R. Measuring transferrin receptor gene expression by NMR imaging. *Biochim Biophys Acta* **1998**; 1402: 239-49. [https://doi.org/10.1016/s0167-4889\(98\)00002-0](https://doi.org/10.1016/s0167-4889(98)00002-0)
16. Zhang Y, Kohler N, Zhang M. Surface modification of superparamagnetic magnetite nanoparticles and their intracellular uptake. *Biomaterials* **2002**; 23: 1553-61. [https://doi.org/10.1016/S0142-9612\(01\)00267-8](https://doi.org/10.1016/S0142-9612(01)00267-8)
17. Fisher B, Costantino JP, Wickerham DL, Redmond CK, Kavanah M, Cronin WM, et al. Tamoxifen for prevention of breast cancer: report of the National Surgical Adjuvant Breast and Bowel Project P-1 Study. *J Natl Cancer Inst* **1998**; 90: 1371-88. <https://doi.org/10.1093/jnci/90.18.1371>
18. Thoidingjam S, Tiku AB. New developments in breast cancer therapy: role of iron oxide nanoparticles. *Adv Nat Sci-Nanosci* **2017**; 8: 023002. <https://doi.org/10.1088/2043-6254/aa5e33>
19. Wu W, He Q, Jiang C. Magnetic iron oxide nanoparticles: synthesis and surface functionalization strategies. *Nanoscale Res Lett* **2008**; 3: 397-415. <https://doi.org/10.1007/s11671-008-9174-9>
20. Bardajee GR, Hooshyar Z. One-pot synthesis of biocompatible

- superparamagnetic iron oxide nanoparticles/hydrogel based on salep: characterization and drug delivery. *Carbohydr Polym* **2014**; 101: 741-51. <https://doi.org/10.1016/j.carbpol.2013.10.028>
21. Wang X, Wei F, Liu A, Wang L, Wang J-C, Ren L, et al. Cancer stem cell labeling using poly (L-lysine)-modified iron oxide nanoparticles. *Biomaterials* **2012**; 33: 3719-32. <https://doi.org/10.1016/j.biomaterials.2012.01.058>
 22. Yilmaz A, Rösch S, Klingel K, Kandolf R, Helluy X, Hiller K-H, et al. Magnetic resonance imaging (MRI) of inflamed myocardium using iron oxide nanoparticles in patients with acute myocardial infarction—preliminary results. *Int J Cardiol* **2013**; 163: 175-82. <https://doi.org/10.1016/j.ijcard.2011.06.004>
 23. Mirsadeghi S, Zandavar H, Yousefi M, Rajabi HR, Pourmortazavi SM. Green-photodegradation of model pharmaceutical contaminations over biogenic Fe₃O₄/Au nanocomposite and antimicrobial activity. *J Environ Manage* **2020**; 270: 110831. <https://doi.org/10.1016/j.jenvman.2020.110831>
 24. Lee N, Hyeon T. Designed synthesis of uniformly sized iron oxide nanoparticles for efficient magnetic resonance imaging contrast agents. *Chem Soc Rev* **2012**; 41: 2575-89. <https://doi.org/10.1039/c1cs15248c>
 25. Bu L, Xie J, Chen K, Huang J, Aguilar ZP, Wang A, et al. Assessment and comparison of magnetic nanoparticles as MRI contrast agents in a rodent model of human hepatocellular carcinoma. *Contrast Media Mol Imaging* **2012**; 7: 363-72. <https://doi.org/10.1002/cmimi.494>
 26. Kohler N, Fryxell GE, Zhang M. A bifunctional poly(ethylene glycol) silane immobilized on metallic oxide-based nanoparticles for conjugation with cell targeting agents. *J Am Chem Soc* **2004**; 126: 7206-11. <https://doi.org/10.1021/ja049195r>
 27. Torchilin VP. *Nanoparticulates as drug carriers*: Imperial college press; **2006**.
 28. Bae KH, Kim YB, Lee Y, Hwang J, Park H, Park TG. Bioinspired synthesis and characterization of gadolinium-labeled magnetite nanoparticles for dual contrast T₁- and T₂-weighted magnetic resonance imaging. *Bioconjug Chem* **2010**; 21: 505-12. <https://doi.org/10.1021/bc900424u>
 29. Gupta AK, Gupta M. Synthesis and surface engineering of iron oxide nanoparticles for biomedical applications. *Biomaterials* **2005**; 26: 3995-4021. <https://doi.org/10.1016/j.biomaterials.2004.10.012>
 30. Kim JE, Shin JY, Cho MH. Magnetic nanoparticles: an update of application for drug delivery and possible toxic effects. *Arch Toxicol* **2012**; 86: 685-700. <https://doi.org/10.1007/s00204-011-0773-3>
 31. Schwaminger SP, García PF, Merck GK, Bodensteiner FA, Heissler S, Günther S, et al. Nature of interactions of amino acids with bare magnetite nanoparticles. *J Phys Chem* **2015**; 119: 23032-41. <https://doi.org/10.1021/acs.jpcc.5b07195>
 32. Pušnik K, Peterlin M, Cigić IK, Marolt G, Kogej K, Mertelj A, et al. Adsorption of amino acids, aspartic acid, and lysine onto iron-oxide nanoparticles. *J Phys Chem* **2016**; 120: 14372-81. <https://doi.org/10.1021/acs.jpcc.6b03180>
 33. Ebrahimezhad A, Ghasemi Y, Rasoul-Amini S, Barar J, Davaran S. Impact of amino-acid coating on the synthesis and characteristics of iron-oxide nanoparticles (IONs). *Bull Korean Chem Soc* **2012**; 33: 3957-62. <https://doi.org/10.5012/bkcs.2012.33.12.3957>
 34. Mazuel F, Espinosa A, Luciani N, Refay M, Le Borgne R, Motte L, et al. Massive intracellular biodegradation of iron oxide nanoparticles evidenced magnetically at single-endosome and tissue levels. *ACS nano* **2016**; 10: 7627-38.
 35. Tie S-L, Lin Y-Q, Lee H-C, Bae Y-S, Lee C-H. Amino acid-coated nano-sized magnetite particles prepared by two-step transformation. *Colloids Surf A Physicochem Eng Asp* **2006**; 273: 75-83. <https://doi.org/10.1016/j.colsurfa.2005.08.027>
 36. Marinescu G, Patron L, Culita DC, Neagoe C, Lepadatu CI, Balint I, et al. Synthesis of magnetite nanoparticles in the presence of aminoacids. *J Nanopart Res* **2006**; 8: 1045-51. <https://doi.org/10.1007/s11051-006-9134-1>
 37. Bonfili L, Cecarini V, Cuccioli M, Angeletti M, Flati V, Corsetti G, et al. Essential amino acid mixtures drive cancer cells to apoptosis through proteasome inhibition and autophagy activation. *FEBS J* **2017**; 284: 1726-37.
 38. Nosrati H, Salehiabar M, Attari E, Davaran S, Danafar H, Manjili HK. Green and one-pot surface coating of iron oxide magnetic nanoparticles with natural amino acids and biocompatibility investigation. *Appl Organomet Chem* **2018**; 32: e4069. <https://doi.org/10.1002/aoc.4069>
 39. Durmus Z, Kavas H, Toprak MS, Baykal A, Altınçekiç TG, Aslan A, et al. L-lysine coated iron oxide nanoparticles: synthesis, structural and conductivity characterization. *J Alloys Compd* **2009**; 484: 371-6. <https://doi.org/10.1016/j.jallcom.2009.04.103>
 40. Ünal B, Durmus Z, Baykal A, Sözeri H, Toprak M, Alpsoy L. L-Histidine coated iron oxide nanoparticles: synthesis, structural and conductivity characterization. *J Alloys Compd* **2010**; 505: 172-8. <https://doi.org/10.1016/j.jallcom.2010.06.022>
 41. Roomi MW, Ivanov V, Kalinovsky T, Niedzwiecki A, Rath M. In vivo and in vitro antitumor effect of ascorbic acid, lysine, proline, arginine, and green tea extract on human fibrosarcoma cells HT-1080. *Med Oncol* **2006**; 23: 105-12.
 42. Couvreur P. Nanoparticles in drug delivery: past, present and future. *Adv Drug Deliv Rev* **2013**; 65: 21-3. <https://doi.org/10.1016/j.addr.2012.04.010>
 43. Nosrati H, Salehiabar M, Davaran S, Danafar H, Manjili HK. Methotrexate-conjugated L-lysine coated iron oxide magnetic nanoparticles for inhibition of MCF-7 breast cancer cells. *Drug Dev Ind Pharm* **2018**; 44: 886-94. <https://doi.org/10.1080/03639045.2017.1417422>
 44. Fard SE, Tafvizi F, Torbati MB. Silver nanoparticles biosynthesised using *Centella asiatica* leaf extract: apoptosis induction in MCF-7 breast cancer cell line. *IET Nanobiotechnol* **2018**; 12: 994-1002. <https://doi.org/10.1049/iet-nbt.2018.5069>
 45. Rahimivand M, Tafvizi F, Noorbazargan H. Synthesis and characterization of alginate nanocarrier encapsulating *Artemisia ciniformis* extract and evaluation of the cytotoxicity and apoptosis induction in AGS cell line. *Int J Biol Macromol* **2020**; 158: 338-57. <https://doi.org/10.1016/j.ijbiomac.2020.05.006>
 46. Yu S, Chow GM. Carboxyl group (-CO₂H) functionalized ferrimagnetic iron oxide nanoparticles for potential bio-applications. *J Mater Chem* **2004**; 14: 2781-6. <https://doi.org/10.1039/b404964k>
 47. Fontana G, Maniscalco L, Schillaci D, Cavallaro G, Giammona G. Solid lipid nanoparticles containing tamoxifen characterization and in vitro antitumoral activity. *Drug Deliv* **2005**; 12: 385-92. <https://doi.org/10.1080/10717540590968855>
 48. Hashem FM, Nasr M, Khairy A. In vitro cytotoxicity and bioavailability of solid lipid nanoparticles containing tamoxifen citrate. *Pharm Dev Technol* **2014**; 19: 824-32. <https://doi.org/10.3109/10837450.2013.836218>
 49. Chan CC. Selective estrogen receptor modulators. *Gynecological Drug Therapy*: CRC Press; **2016**. p. 105-10.
 50. Pérez E, Benito M, Teijón C, Olmo R, Teijón JM, Blanco MD. Tamoxifen-loaded nanoparticles based on a novel mixture of biodegradable polyesters: characterization and in vitro evaluation as sustained release systems. *J Microencapsul* **2012**; 29: 309-22. <https://doi.org/10.3109/02652048.2011.651496>
 51. Blanco MD, Guerrero S, Benito M, Teijón C, Olmo R, Muniz E, et al. Tamoxifen-loaded folate-conjugate poly [(p-nitrophenyl acrylate)-co-(N-isopropylacrylamide)] sub-microgel as antitumoral drug delivery system. *J Biomed Mater Res A* **2010**; 95: 1028-40. <https://doi.org/10.1002/jbm.a.32929>
 52. Steller H. Mechanisms and genes of cellular suicide. *Science* **1995**; 267: 1445-9. <https://doi.org/10.1126/science.7878463>
 53. Voltairas PA, Fotiadis DI, Michalis LK. Hydrodynamics of magnetic drug targeting. *J Biomech* **2002**; 35: 813-21. [https://doi.org/10.1016/s0021-9290\(02\)00034-9](https://doi.org/10.1016/s0021-9290(02)00034-9)
 54. Sharma G, Kodali V, Gaffrey M, Wang W, Minard KR, Karin NJ, et al. Iron oxide nanoparticle agglomeration influences dose rates and modulates oxidative stress-mediated dose-response profiles in vitro. *Nanotoxicology* **2014**; 8: 663-75. <https://doi.org/10.3109/174>

- 35390.2013.822115
55. Nomani A, Nosrati H, Manjili HK, Khesalpour L, Danafar H. Preparation and Characterization of Copolymeric Polymersomes for Protein Delivery. *Drug Res (Stuttg)* **2017**; 67: 458-65. <https://doi.org/10.1055/s-0043-106051>
 56. Salehiabar M, Nosrati H, Davaran S, Danafar H, Manjili HK. Facile Synthesis and Characterization of L-Aspartic Acid Coated Iron Oxide Magnetic Nanoparticles (IONPs) For Biomedical Applications. *Drug Res (Stuttg)* **2018**; 68: 280-5. <https://doi.org/10.1055/s-0043-120197>
 57. Arias JL, Gallardo V, Gomez-Lopera SA, Plaza RC, Delgado AV. Synthesis and characterization of poly(ethyl-2-cyanoacrylate) nanoparticles with a magnetic core. *J Control Release* **2001**; 77: 309-21. [https://doi.org/10.1016/s0168-3659\(01\)00519-3](https://doi.org/10.1016/s0168-3659(01)00519-3)
 58. Maeda H, Wu J, Sawa T, Matsumura Y, Hori K. Tumor vascular permeability and the EPR effect in macromolecular therapeutics: a review. *J Control Release* **2000**; 65: 271-84. [https://doi.org/10.1016/s0168-3659\(99\)00248-5](https://doi.org/10.1016/s0168-3659(99)00248-5)
 59. Nomura T, Koreeda N, Yamashita F, Takakura Y, Hashida M. Effect of particle size and charge on the disposition of lipid carriers after intratumoral injection into tissue-isolated tumors. *Pharm Res* **1998**; 15: 128-32. <https://doi.org/10.1023/A:1011921324952>
 60. Gautier J, Allard-Vannier E, Munnier E, Souce M, Chourpa I. Recent advances in theranostic nanocarriers of doxorubicin based on iron oxide and gold nanoparticles. *J Control Release* **2013**; 169: 48-61. <https://doi.org/10.1016/j.jconrel.2013.03.018>
 61. Zhang H, Wang C, Chen B, Wang X. Daunorubicin-TiO₂ nanocomposites as a "smart" pH-responsive drug delivery system. *Int J Nanomedicine* **2012**; 7: 235. <https://doi.org/10.2147/IJN.S27722>
 62. Xing R, Bhirde AA, Wang S, Sun X, Liu G, Hou Y, et al. Hollow iron oxide nanoparticles as multidrug resistant drug delivery and imaging vehicles. *Nano Res* **2013**; 6: 1-9. <https://doi.org/10.1007/s12274-012-0275-5>
 63. Bhirde AA, Kapoor A, Liu G, Iglesias-Bartolome R, Jin A, Zhang G, et al. Nuclear mapping of nanodrug delivery systems in dynamic cellular environments. *ACS Nano* **2012**; 6: 4966-72. <https://doi.org/10.1021/nn300516g>
 64. Prabha G, Raj V. Synthesis and characterization of chitosan-polyvinylpyrrolidone-bovine serum albumin-coated magnetic iron oxide nanoparticles as potential carrier for delivery of tamoxifen. *J Iran Chem Soc* **2018**; 15: 871-84. <https://doi.org/10.1007/s13738-017-1286-7>
 65. Hu FX, Neoh KG, Kang ET. Synthesis and in vitro anti-cancer evaluation of tamoxifen-loaded magnetite/PLLA composite nanoparticles. *Biomaterials* **2006**; 27: 5725-33. <https://doi.org/10.1016/j.biomaterials.2006.07.014>
 66. Majd MH, Asgari D, Barar J, Valizadeh H, Kafil V, Abadpour A, et al. Tamoxifen loaded folic acid armed PEGylated magnetic nanoparticles for targeted imaging and therapy of cancer. *Colloids Surf B Biointerfaces* **2013**; 106: 117-25. <https://doi.org/j.colsurfb.2013.01.051>
 67. Akim AM, Tung EE, Chong PP, Hamzah MY, Dahlan KZM, editors. Nanoparticle-Encapsulated Tamoxifen Inducing Cytotoxic Effect on MCF-7 Breast Cancer Cell Lines. Berlin, Heidelberg: Springer; **2013**.
 68. Mohanty C, Sahoo SK. The in vitro stability and in vivo pharmacokinetics of curcumin prepared as an aqueous nanoparticulate formulation. *Biomaterials* **2010**; 31: 6597-611. <https://doi.org/j.biomaterials.2010.04.062>
 69. Abbasi S, Paul A, Shao W, Prakash S. Cationic albumin nanoparticles for enhanced drug delivery to treat breast cancer: preparation and in vitro assessment. *J Drug Deliv* **2012**; 2012: 686108. <https://doi.org/10.1155/2012/686108>
 70. Cavallaro G, Maniscalco L, Licciardi M, Giammona G. Tamoxifen-loaded polymeric micelles: preparation, physico-chemical characterization and in vitro evaluation studies. *Macromol Biosci* **2004**; 4: 1028-38. <https://doi.org/10.1002/mabi.200400089>
 71. Roy PG, Thompson AM. Cyclin D1 and breast cancer. *Breast* **2006**; 15: 718-27. <https://doi.org/10.1016/j.breast.2006.02.005>
 72. Chawla JS, Amiji MM. Cellular uptake and concentrations of tamoxifen upon administration in poly(epsilon-caprolactone) nanoparticles. *AAPS PharmSci* **2003**; 5: E3. <https://doi.org/10.1208/050203>
 73. Osborne CK, Bardou V, Hopp TA, Chamness GC, Hilsenbeck SG, Fuqua SA, et al. Role of the estrogen receptor coactivator AIB1 (SRC-3) and HER-2/neu in tamoxifen resistance in breast cancer. *J Natl Cancer Inst* **2003**; 95: 353-61. <https://doi.org/10.1093/jnci/95.5.353>
 74. Hurtado A, Holmes KA, Geistlinger TR, Hutcheson IR, Nicholson RI, Brown M, et al. ERBB2 regulation by estrogen receptor-Pax2 determines tamoxifen response. *Nature* **2008**; 456: 663. <https://doi.org/10.1038/nature07483>
 75. Mazumdar S, Italiya KS, Sharma S, Chitkara D, Mittal A. Effective cellular internalization, cell cycle arrest and improved pharmacokinetics of Tamoxifen by cholesterol based lipopolymeric nanoparticles. *Int J Pharm* **2018**; 543: 96-106. <https://doi.org/10.1016/j.ijpharm.2018.03.022>
 76. Abbasalipourkabir R, Salehzadeh A, Abdullah R. Tamoxifen-loaded solid lipid nanoparticles-induced apoptosis in breast cancer cell lines. *J Exp Nanosci* **2016**; 11: 161-74. <https://doi.org/10.1080/17458080.2015.1038660>